ACS OMEGA

http://pubs.acs.org/journal/acsodf

Article

Magnetic Control of the Manganese Photoluminescence in Fe_3O_4/L-Cys ZnS:Mn Nanocomposites

Shyam Sutariya, Mohammed Bsatee, Olesia Gololobova, Daysi Diaz-Diestra, Bibek Thapa, Brad R. Weiner, Gerardo Morell, Wojciech M. Jadwisienczak, and Juan Beltran-Huarac*

Cite This: *ACS Omega* 2021, 6, 7598−7604

Read Online

ACCESS | Metrics & More | Article Recommendations | Supporting Information

ABSTRACT: We investigated the magnetic control of the Mn photoluminescence (PL) in iron oxide/L-cysteine-capped zinc sulfide (Fe_3O_4/L-cys ZnS:Mn) nanocomposites via temperature- and field-dependent PL intensity studies. Fe_3O_4/L-cys ZnS:Mn was synthesized following a wet chemical deposition route and then its physicochemical, morphological, and magnetic properties were characterized. X-ray diffraction analysis indicates the formation of a semiconducting composite material with coexisting phases with high crystalline quality and purity. Electron microscopy reveals that the surfaces of the nanoparticles are clean and smooth, sized between 15 and 30 nm, without any sheathed amorphous phase. Vibrating sample magnetometry and UV light excitation show a clear superparamagnetic behavior and an optical response of Fe_3O_4/L-cys ZnS:Mn, which revealed its bifunctional nature. Magnetoluminescent coupling at 1.0 T is seen in the form of PL suppression in Fe_3O_4/L-cys ZnS:Mn from low temperature (10 K) to room temperature, with a PL intensity drop of ∼5% at 10 K and a maximum drop of 10% at room temperature. This observation can be explained by restriction of the energy transfer to Mn orbitals through magnetic ordering and Jahn−Teller distortions. Fe_3O_4/L-cys ZnS:Mn shows promise as a bifunctional biocompatible compound that can be applied as a theranostic agent and a quantum computational element. A deeper understanding behind the magnetic control of the optical response in bifunctional materials brings forth new arenas in diagnostics and drug delivery.

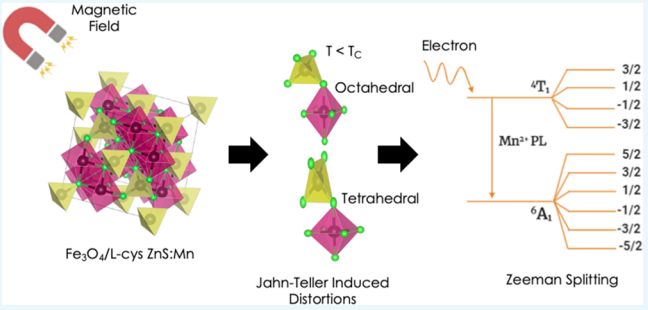

INTRODUCTION

Various research initiatives for producing new tools to advance magnetoluminescent (ML) technology have led to widespread attention on diluted magnetic semiconductors (DMSs).[1−4] DMSs exhibit unique properties, offering ample opportunities for designing photonic devices with tunable functionalities.[5] Doping of transition metal ions into DMSs induces the hybridization of sp levels of host matrixes with the d orbitals of impurities, whose degeneracy is lifted by Zeeman splitting.[6,7] Such a hybridization along with itinerant carriers may trigger interactions between localized d orbitals (e.g., double or super exchange), anion vacancies, and lattice cores. As a result, different magnetic orderings (paramagnetism, superparamagnetism, ferromagnetism, or antiferromagnetism) are established depending on the strength of the d−d and the d−sp exchange interactions.[8−11] In this sense, new optical, magnetic, and ML responses may be tuned by surface modification and depletion of shallow luminescent centers. To date, only a few reports that elucidate the hybridization mechanism in magneto-optics have been documented.[12−14]

Nanostructured zinc sulfide (ZnS) doped slightly (i.e., ≤5%) with manganese (ZnS:Mn) has been studied due to its lifetime shortening and high photoluminescence (PL) efficiency, ascribed to the prominent exchange interaction between the sp band electrons of ZnS and the d electrons of Mn^{2+} ions.[15−20] Recent challenges in ZnS:Mn focus on better understanding the mechanism by which the spin-forbidden $^4T_1-^6A_1$ transition of manganese becomes less spin forbidden, which would in turn bring about faster energy transfer via orbital hybridization.[15,16,21] It has been reported that ZnS:Mn (doping ≤ 5%) exhibits ferromagnetic ordering below 30 K,[15,16,20] which is associated with both the movement of the d-level within the host lattice and the degree of disorder due to its low dimensionality.[22] Sarkar et al. reported that the ferromagnetic ordering-induced spin-sensitive energy transfer to Mn-states in ZnS:Mn can produce a significant drop of emission band PL intensity at high magnetic fields (20−50 T).[15,20] More recently, our group reported that the internal orange emission transition in ferromagnetically ordered

Received: December 17, 2020
Accepted: March 2, 2021
Published: March 10, 2021

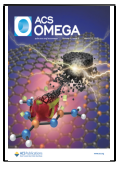

ZnS:Mn is stable when exposed to low magnetic fields (∼1 T).[16] No ML coupling was reported in its paramagnetic phase, between 40 and 90 K.[16] In a separate account, we showed that a surface modification of ZnS:Mn with a surrounding magnetic perovskite matrix induced a ML response at moderate temperatures of up to 225 K at 1 T. This was explained by evoking a magnetic ordering-induced spin-dependent restriction of the energy transfer to Mn states.[21] L-Cysteine-capped nano-ZnS was applied as a fluorescence probe for protein detection.[23] Recently, we employed L-cysteine-capped ZnS:Mn quantum dots as probes for dopamine detection.[17] Nonetheless, rare earth-free ZnS:Mn systems capable of activating spin-dependent restrictions upon surface modification remain still unsettled.

We report here a comprehensive study on the magnetic control of the Mn PL in iron oxide (Fe_3O_4)/L-cysteine-capped ZnS:Mn (Fe_3O_4/L-cys ZnS:Mn) nanocomposites. Fe_3O_4, used as the biocompatible matrix for ZnS:Mn, exhibits a superparamagnetic response at room temperature (RT).[24] The synthesis and material properties of Fe_3O_4/L-cys ZnS:Mn are studied along with its optical response. The orange emission tunability of the nanocomposite stems from L-cys ZnS:Mn, obtained from temperature- and field-dependent studies, and indicates that ML coupling takes place even at temperatures higher than that of the ferromagnetic ordering when exposed to low magnetic fields.

RESULTS AND DISCUSSION

The optimized Fe_3O_4/L-cys ZnS:Mn product was synthesized via wet chemical routes and manufactured into powder and pellet forms for characterization. Quality control inductively coupled plasma (ICP) elemental analysis revealed that the composition of the compound contains 15.3% w/w Fe_3O_4, 19.8% w/w ZnS, and 1.7% w/w of Mn (11.1% of Fe and 13.3% of Zn). To study the structure, crystallinity, phase, and size of the products, we conducted X-ray diffraction (XRD). The XRD pattern of Fe_3O_4/L-cys ZnS:Mn (Fe_3O_4 and L-cys ZnS:Mn are also included for comparison) is depicted in Figure 1. The diffraction peaks observed were indexed to the

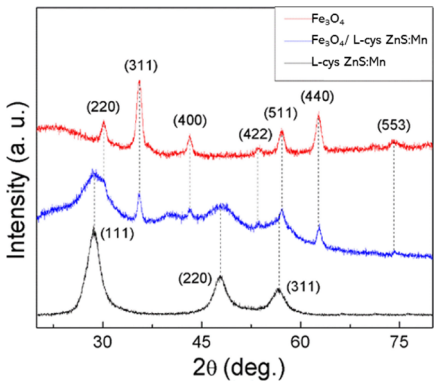

Figure 1. XRD patterns of the Fe_3O_4/L-cys ZnS:Mn nanocomposites and the Fe_3O_4 and L-cys ZnS:Mn NPs.

diffraction planes of the cubic sphalerite ZnS phase [(111), (220), and (311)] and the cubic inverse spinel Fe_3O_4 phase [(220), (311), (400), (422), (511), (440), and (553)], in accordance with the JCPDS no. 77-2100 and JCPDS no. 79-0418 cards, respectively.[24−27] The observed well-defined peaks, the absence of mix-valence phases (including Fe_2O_3 and ZnO) in the XRD pattern, and the coexistence of both phases evidently suggest the formation of the semiconducting and composite materials with high crystalline quality and purity. Note that there is a small but noticeable peak between the (311) and (400) diffraction peaks. Because the peak is not well-defined and very low in intensity (basically at the level of the signal-to-noise ratio), the peak is presumably related to a secondary or parasitic phase typical in iron-based nanocomposites. The broadening of the diffraction peaks is ascribed to the nanocrystalline nature of the particles. Their average crystallite size was calculated using Scherrer's formula, yielding ∼11 nm for Fe_3O_4/L-cys ZnS:Mn. Similar calculations yield ∼3 nm for L-cys ZnS:Mn and ∼8 nm for Fe_3O_4. It was also observed that the diffraction peaks of Fe_3O_4/L-cys ZnS:Mn were relatively shifted (and consequently overlapped) when compared to those of bare Fe_3O_4 and L-cys ZnS:Mn. This is due to the internal strain between both phases developed during the synthesis conditions, and to the lattice mismatch.[21,28]

To further confirm the size of the nanoparticles (NPs), and determine their morphology and degree of abundance, transmission electron microscopy (TEM) was conducted by dispersing the NPs onto carbon grids. TEM images of Fe_3O_4/L-cys ZnS:Mn nanocomposites (L-cys ZnS:Mn and Fe_3O_4 are also shown for comparison) are depicted in Figure 2. It was observed that the Fe_3O_4/L-cys ZnS:Mn nanocomposites form some thin clusters with minor void volumes (Figure 2b). From the gray scale contrasts, they appear to be composed of small crystalline NPs formed by two different constituents (Figure 2a,c). In general, the surfaces of individual particles are clean and smooth without any sheathed amorphous phase, which indicates that our synthesis method provides a low degree of interdiffusion between Fe_3O_4 and L-cys ZnS:Mn and the surrounding medium. The NP size was determined to be 22 ± 8 nm, consistent with that estimated from XRD analysis. It should be noted that the electron beam illumination did not cause any increase of planar induced phase transformation or amorphous carbon deposition. The polycrystalline nature of the nanocomposite was corroborated via selected area electron diffraction as shown in the inset of Figure 2b.

To evaluate whether Fe_3O_4/L-cys ZnS:Mn inherited the intrinsic magnetic properties of Fe_3O_4 cores, vibrating sample magnetometry (VSM) was performed on each type of NP at RT. The M−H curves of bare Fe_3O_4 and Fe_3O_4/ZnS:Mn collected at RT are depicted in Figure 3. The curves show that Fe_3O_4 exhibits a high saturation magnetization (M_S) of 71.5 emu g^{-1}, negligible coercivity (H_C), and almost-zero remnant field (M_R, very low volume anisotropy). Along with the fact that Fe_3O_4 is rapidly magnetized when exposed to an external magnetic field, it provides clear indication that Fe_3O_4 is superparamagnetic, consistent with the single-domain superparamagnetic criteria in this size regime (average core size < 20 nm).[25] When compared to Fe_3O_4, Fe_3O_4/L-cys ZnS:Mn shows a similar magnetic trend that arises from the superparamagnetic cores.[29,30] Fe_3O_4/L-cys ZnS:Mn possesses a saturation magnetization of 36.5 emu g^{-1}. The decrease in observed M_S (∼45% compared to Fe_3O_4) is ascribed to the charge transfer change caused by the interaction between L-cys ZnS:Mn and Fe_3O_4,[31−33] and to the dielectric ordering coupled to the superparamagnetic phase that acts as voids or pores in the presence of an external magnetic field. These effects disrupt the magnetic circuits thus resulting in a significant drop of M_S.[31] A reduction of M_R and H_C from

https://dx.doi.org/10.1021/acsomega.0c06164
ACS Omega 2021, 6, 7598−7604

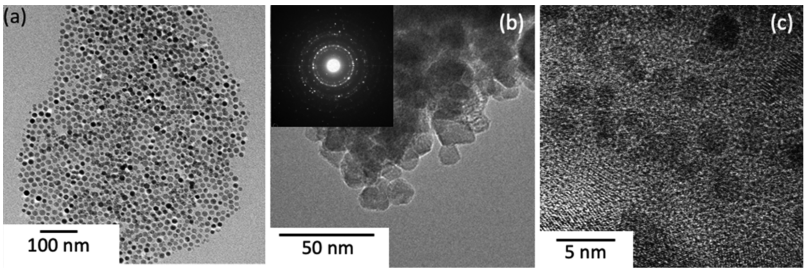

Figure 2. Bright-field TEM images of (a) Fe_3O_4 NPs, (b) Fe_3O_4/L-cys ZnS:Mn nanocomposites (the inset shows the selected area electron diffraction pattern of Fe_3O_4/L-cys ZnS:Mn), and (c) L-cys ZnS:Mn NPs.

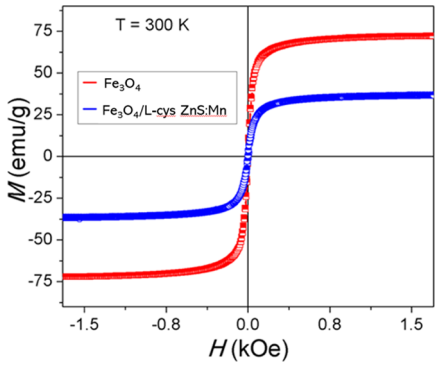

Figure 3. $M-H$ curves of Fe_3O_4 and Fe_3O_4/L-cys ZnS:Mn.

1.75 to 0.63 emu g^{-1} and from $\mu_o H_C$ = 2.33 to 1.53 mT, respectively, was observed when L-cys ZnS:Mn is incorporated with Fe_3O_4.

We conducted temperature-dependent PL spectroscopy on Fe_3O_4/L-cys ZnS:Mn. Figures 4a and S1 shows the PL response as a function of temperature for Fe_3O_4/L-cys ZnS:Mn and L-cys ZnS:Mn taken after two cycles of temperature measurement, respectively. On average, the respective PL intensities (as seen in Figure 4b) showed an intensity suppression for Fe_3O_4/L-cys ZnS:Mn when compared to L-cys ZnS:Mn in all ranges of temperatures. This effect is ascribed to the presence of Fe_3O_4, which acts similar to activated impurities. This process changes surface defect (vacancy) states for energy transfer that in turn reduce the influence of Mn^{2+}. The whole effect results in lowering the amount of $^4T_1-{}^6A_1$ transitions.[29,34]

We have studied the ML effect of Fe_3O_4/L-cys ZnS:Mn in the presence and absence of an external magnetic field (1.0 T) in the temperature range of 10−300 K. ML measurements were performed by applying a static magnetic field on the longitudinal plane of Fe_3O_4/L-cys ZnS:Mn, above and below its superparamagnetic ordering temperature. Prominent and reproducible ML coupling was observed at various temperature ranges, as depicted in Figure 5.

A noticeable drop in the ML intensity for the Fe_3O_4/L-cys ZnS:Mn was observed from low temperature (LT) (10 K) to RT. The calculated percentage difference of the PL intensity between zero field and 1.0 T at 10 K was ∼4.5%, which reached a peak value of ∼10% at 300 K. This quenching correlates well with the changes in the PL spectra under zero field, attributed to the charge transfer change caused by the interaction of Fe_3O_4 with L-cys ZnS:Mn.[14] The ML-quenching mechanism is ascribed to the photoinduced electron transfer between the conducting and valence bands (Figure 6). ZnS:Mn containing NPs exhibit a characteristic band, an internal Mn^{2+} ion transition between the $^4T_1$ first excited state (spin 3/2) and the $^6A_1$ ground state (spin 5/2).[16,21] It results in a unique energy transfer pathway in which the exciton flows from the s−p electron−hole pair band states (host ZnS) to the Mn^{2+} ion d-electron states rather than the ground state, leading to a broad orange emission band centered at ∼598 nm (Figure 6c).[16] When Fe_3O_4 is linked to create the bifunctional nanocomposite, the energy transfer pathway is disrupted.[29,33,35,36] In the absence of a magnetic field, the PL

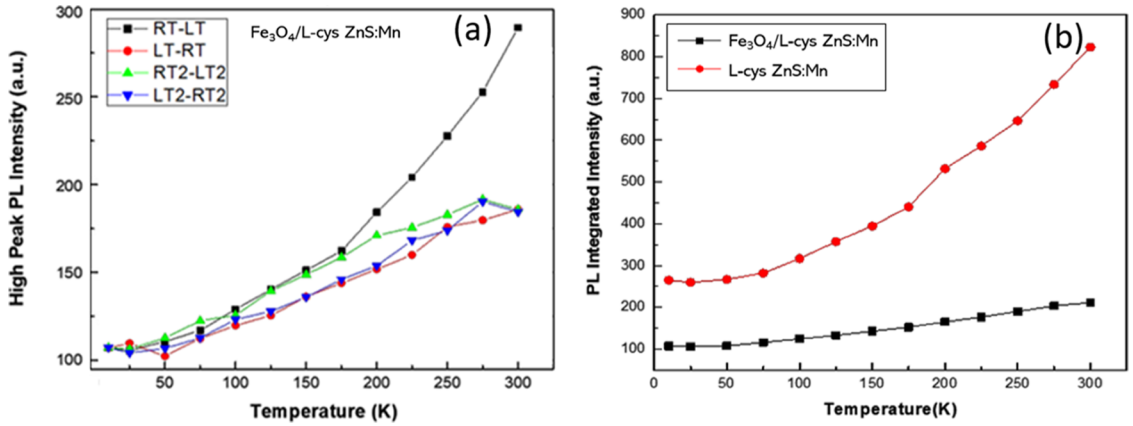

Figure 4. (a) Maximum PL intensity of the orange emission band (598 nm) as a function of temperature of Fe_3O_4/L-cys ZnS:Mn at 325 nm excitation and zero field. PL spectra were collected following the sequence: (1) sample was cooled from RT to LT, (2) sample was warmed up from LT to RT, (3) sample was cooled down from RT to LT, and (4) sample was warmed up from LT to RT. (b) Averaged PL intensities of L-cys ZnS:Mn and Fe_3O_4/L-cys ZnS:Mn in zero field.

https://dx.doi.org/10.1021/acsomega.0c06164
ACS Omega 2021, 6, 7598−7604

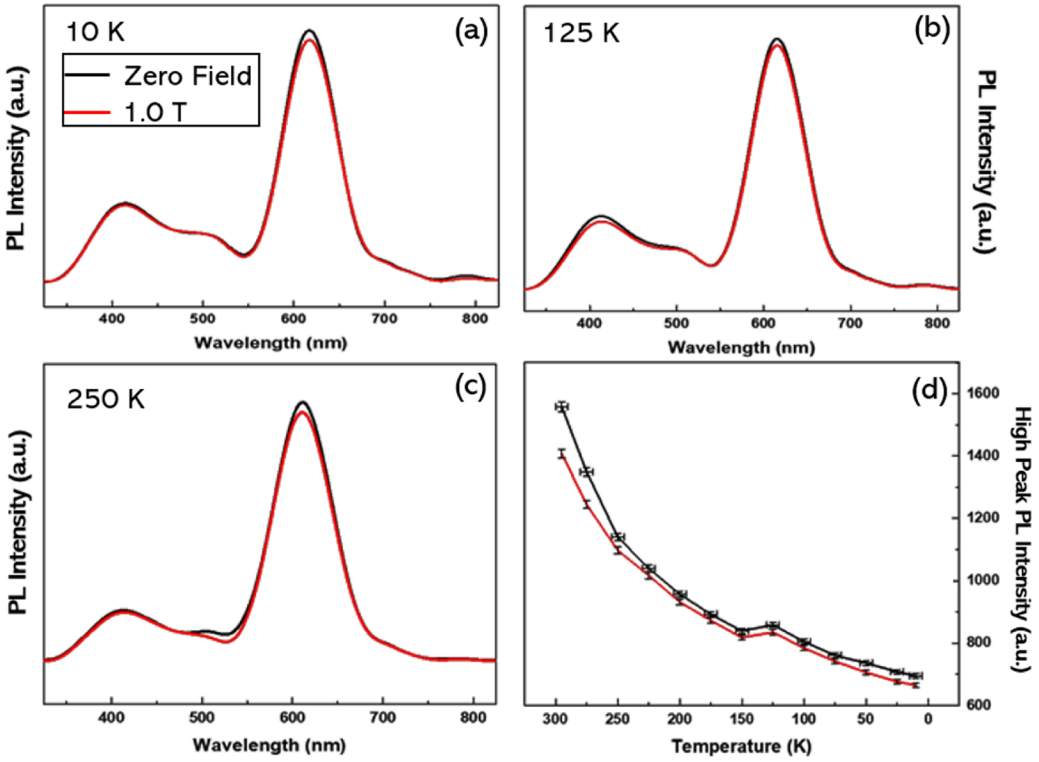

Figure 5. (a−c) PL spectra of the Fe_3O_4/L-cys ZnS:Mn nanocomposites at 10, 125, and 250 K in the absence and presence of an external magnetic field (1.0 T). (d) High peak PL intensity as a function of temperature of Fe_3O_4/L-cys ZnS:Mn in the absence and presence of an external magnetic field (1.0 T).

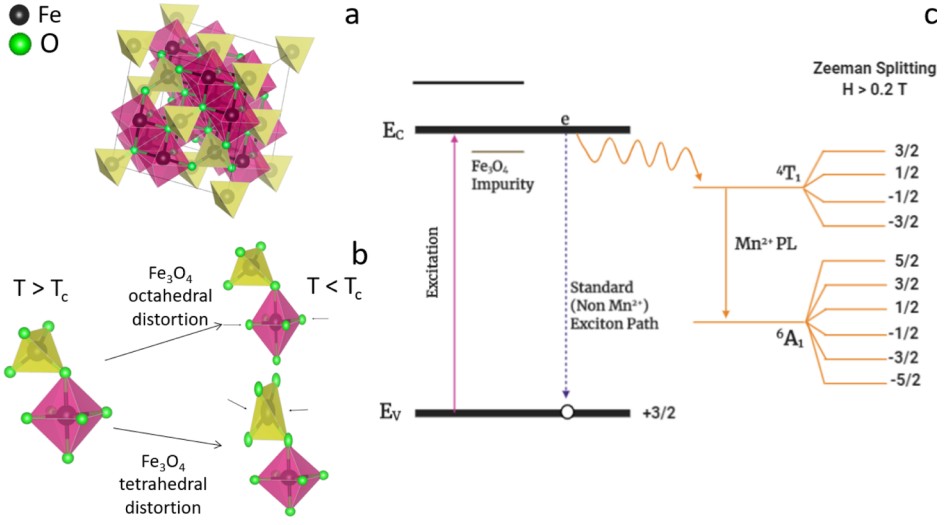

Figure 6. (a) Inverse spinel lattice structure of Fe_3O_4 (magnetite). (b) Tetrahedral and octahedral distortion of Fe_3O_4. (c) Mechanism of the internal Mn-PL transition of Fe_3O_4/L-cys ZnS:Mn restricted by magnetic-ordering-induced spin dependence.

suppression is due to the inherent nature of adding impurities to a lattice. The Fe_3O_4 in Fe_3O_4/L-cys ZnS:Mn provides vacancies in which the excitons may flow to rather than the Mn^{2+} band, lowering the number of $^4T_1$−$^6A_1$ transitions and leading to a decrease of recombinant photons and PL intensity.[29,37] Further suppression, due to ML coupling, may be a result of ordering within magnetic domains. When magnetic domains within the nanocomposite are oriented in a nonsuperparamagnetic fashion the PL intensity might drop. The exposure to a magnetic field (>0.2 T) is known to induce Zeeman splitting, splitting the d-electron orbitals of Mn from 5 to 10 (4 for the first excited state and 6 for the ground state) nondegenerate orbitals.[15] The magnetic ordering can result in spin polarization, which would limit the pathway that excitons are able to take from within the internal split Mn bands (Figure 6c). In this sense, less excitons could flow from $^4T_1$ to $^6A_1$, instead opting for the more energetically favored spin-restricted transitions, resulting in less photons being emitted. In addition, the structure may have also an effect on the PL intensity. The magnetic matrix (Fe_3O_4) within the nanocomposite has an inverse spinel lattice structure.[38] This means that there are both tetrahedral and octahedral domains within

https://dx.doi.org/10.1021/acsomega.0c06164
ACS Omega 2021, 6, 7598−7604

the lattice, each able to undergo their own Jahn−Teller distortions (Figure 6a,b). Nonlinear molecules (including Fe_3O_4) undergo geometric distortions to lower the overall energy by removing degeneracy, resulting in spin polarization.[39] These distortions are also able to block the flow of excitons due to further spin polarization, resulting in less photon emission[21] Nonetheless, further studies are needed to better understand the dynamics of excitonic complexes at which magnetic ordering shifts for Fe_3O_4/L-cys ZnS:Mn and other bifunctional biocompatible nanosystems.

CONCLUSIONS

We have produced bifunctional nanocomposites to remotely control their orange emission by applying an external magnetic field. Biocompatible Fe_3O_4/L-cys ZnS:Mn nanocomposites were synthesized via a wet chemical deposition route using bare iron oxide NPs as seeds to grow L-cys ZnS:Mn NPs. Physicochemical characterization indicates that the nanocomposites exhibit high crystalline quality and purity with a superparamagnetic response arising from magnetite and orange emission from L-cys ZnS:Mn. It is proposed that the internal transition of excitons from the conduction band to the Mn states is disrupted by the presence of Fe_3O_4. Paired with a magnetic field that causes Zeeman splitting, the spin-selective energy transfer is also compromised. Jahn−Teller distortions may lower the overall energy by also removing degeneracy resulting in spin polarization, which is able to block the flow of excitons due to further spin polarization. The results presented here help explain the underlying factors contributing to the ML properties of bifunctional nanocomposites, and reveals the potential of Fe_3O_4/L-cys ZnS:Mn as a bifunctional compound whose optical properties can be remotely adjusted, which is suitable for theranostics, magneto-optics, spintronics, and nanoelectronics.

EXPERIMENTAL SECTION

Materials. Hexane (anhydrous, 95%), ethyl alcohol (EtOH), oleic acid (OA, 99%), tri-*n*-octylamine (TOA, >98.0%), and sodium oleate (NaOL, >97.0%) were purchased from Alfa Aesar. Sodium hydroxide (NaOH), iron(III) chloride hexahydrate ($FeCl_3{\cdot}6H_2O$, 97.0−102.0%), zinc sulfate monohydrate ($ZnSO_4{\cdot}H_2O$), manganese chloride tetrahydrate ($MnCl_2{\cdot}4H_2O$), sodium sulfide (Na_2S), and L-cysteine were purchased from Sigma-Aldrich and were used without further purification.

Synthesis of L-Cys ZnS:Mn NPs. L-Cys ZnS:Mn was synthesized via an inorganic wet chemical approach reported previously by our research group.[16,17,40] In general, 90 mg of $ZnSO_4$, 3 mg of $MnCl_2$, and 121 mg of L-cysteine were dissolved in high-purity deionized (DI) water. The pH of the resulting mixture was adjusted to 11 using 1 M NaOH. 5 mL of 0.2 M aqueous solution of Na_2S was gradually added in the presence of argon, then stirred under reflux for 14 h at 50 °C in open air. The collected NPs were purified by ultracentrifugation followed by thorough rinsing with water, and then freeze-dried to obtain the final product in the powder form. Adding L-cysteine to the surface of ZnS:Mn provides more dispersibility in aqueous solution minimizing particle aggregation, which in turn can prevent fluorescence quenching due to nonspecific binding.[23,41]

Synthesis of Fe_3O_4 NPs. Fe_3O_4 was synthesized via thermal decomposition reported previously by our research group with minor modifications.[25] Briefly, OA (1.5 mmol) and iron oleate (3 mmol) were dissolved in TOA (45 mL) through bath sonication. The solution was degassed for 30 min in the presence of nitrogen, and then aged at 340 °C (a heating rate of 10 °C/min up to 340 °C) for 2 h. The final product was allowed to cool down to RT before being collected as the pellet via centrifugation. The pellet was freeze-dried and then used in part for further synthesis procedures and characterization.

Synthesis of Fe_3O_4/L-Cys ZnS:Mn Nanocomposites. Fe_3O_4/L-cys ZnS:Mn was synthesized following a wet chemical deposition route.[21,26] Bare iron oxide NPs were used as seeds, and suspended in 85 mL of DI H_2O at a concentration of 0.05 M. Then, 5 mL of the L-cysteine solution (0.1 M), 5 mL of the $ZnSO_4$ solution (2 M), and 5 mL of $MnCl_2$ (1 M) were gradually added and stirred vigorously for 10 min. To deprotonate the thiol groups of L-cysteine so they could anchor the Zn^{2+} and Mn^{2+} sites onto the surface of seed cores, the pH of the solution was increased to 11 by adding 1 M NaOH. The solution was then purged with N_2 for 30 min before 10 mL of the Na_2S solution (1.1 M) was injected to the flask. The solution was then aged at 50 °C for 2 h. Ultracentrifugation was then used to remove the flocculate. After redispersion in DI H_2O and ethanol, the resulting solution was further centrifuged before being magnetically collected, vigorously rinsed, and freeze-dried.

Mass Spectrometry Analysis. Actual elemental composition was measured via ICP−mass spectrometry (ICP−MS) analysis using a NexION 300D ICP mass spectrometer (PerkinElmer, USA) equipped with SC4-DX autosamplers (ESI, USA). Decomposition of the samples' matrix was performed by heating at 70 °C for 16 h after the addition of trace metal grade nitric acid (20% aqueous solution). Digested samples were diluted (1:10) with pico-pure water and with 2% nitric acid to fit into the calibration curve. ICP−MS was operated in standard mode, all operating parameters were optimized to meet requirements as defined by the manufacturer prior to method calibration and analysis. Calibration curves were constructed using a five-point calibration curve in a range 10−1000 ppb for Fe and 0.1−10 ppb for Zn and Mn. Five replicates were analyzed per sample. Quantification was performed by germanium as an internal standard.

Structural and Magnetic Characterization. The phase and crystallinity of Fe_3O_4, L-cys ZnS:Mn, and Fe_3O_4/L-cys ZnS:Mn were analyzed from diffractograms recorded using a SmartLab powder X-ray diffractometer (Rigaku Corporation) equipped with a Cu Kα radiation source (λ = 1.5406 Å) operating at an accelerating potential of 40 kV and a tube current of 44 mA. The size, surface morphology, and degree of abundance were studied from micrographs using a Carl Zeiss Leo 922 transmission electron microscope. The RT magnetic properties were studied using a vibrating sample magnetometer (Lakeshore 7400).

Optical Characterization. The temperature-dependent PL data were collected using a procedure reported elsewhere.[16,21] The NPs in the pellet form were mounted on the cold-finger of a closed-cycle helium-cryostat operating from 10 to 320 K under high vacuum conditions (<0.1 mPa). The samples were then excited with a 325 nm He−Cd laser (model IK 3202R-D) with a maximum power of 3.2 mW mm^{-2}. The PL signal was dispersed using a 0.3 m Acton spectrometer with changeable holographic gratings and analyzed using a Princeton Instrument PI-MAX charge-coupled device camera

https://dx.doi.org/10.1021/acsomega.0c06164
ACS Omega 2021, 6, 7598−7604

equipped with a UV intensifier, operating in the spectral region of 200−950 nm.

ML Measurements. ML spectra were recorded by placing the samples onto the cold stage of a closed-cycle cryostat (model 202-E) coupled to an electromagnet (Lake Shore, model EM4-HVA). First, the system was evacuated followed by the temperature setting. The magnetic field strength was monitored with a Gauss meter probe (Lake Shore, model 475-DSP). The long-term magnetic field stability was 0.001 T, and no magnetic field strength drift was observed during data collection (∼5−10 min). The temperature was monitored using a temperature controller (Lake Shore 340) with a stability of ±0.5 K. The samples were excited with a 325 nm He−Cd laser (Model IK 3202R-D) with an excitation power density of 2.6 mW mm^{-2}. The optical signal was collected using a fiber optic spectrometer (Ocean Optics, model USB2000+). Different optical filters were used along the optical detection path to selectively record luminescence from studied specimens. Typically, spectra were measured only at selected temperatures. Samples were magnetized individually after a specimen reached a temperature set point. During temperature change cycles, between different set points, the magnetic field was turned off. As the temperature was set and stabilized, the sample underwent two temperature cycles. A temperature cycle is defined as the process of cooling the sample from RT to LT or the process of warming the sample from LT to RT. Consequently, a 2-cycle measurement is the temperature change from RT(1) to LT(1), LT(1) to RT(1), and RT(2) to LT(2), and finally LT(2) to RT(2). Extra precautions in experimental error/drag were taken into account to eliminate laser beam intensity drift (±0.001 mW), cryostat temperature fluctuations (±0.5 K), and to provide external magnetic field stability (±10 Oe) over >60 min.

■ ASSOCIATED CONTENT

Supporting Information

The Supporting Information is available free of charge at https://pubs.acs.org/doi/10.1021/acsomega.0c06164.

> Maximum PL intensity of the orange emission band (598 nm) as a function of temperature of L-cys ZnS:Mn at 325 nm excitation and zero fields (PDF)

■ AUTHOR INFORMATION

Corresponding Author

Juan Beltran-Huarac − *Department of Physics, East Carolina University, Greenville, North Carolina 27858, United States;* orcid.org/0000-0003-3423-0114; Email: beltranhuaracj19@ecu.edu

Authors

Shyam Sutariya − *Neuroscience Program, Department of Psychology, East Carolina University, Greenville, North Carolina 27858, United States*

Mohammed Bsatee − *School of Electrical Engineering and Computer Science, Ohio University, Athens, Ohio 45701, United States*

Olesia Gololobova − *Center for Nanotechnology in Drug Delivery, Eshelman School of Pharmacy, University of North Carolina at Chapel Hill, Chapel Hill, North Carolina 27599, United States;* orcid.org/0000-0002-0392-268X

Daysi Diaz-Diestra − *Department of Chemistry, University of Puerto Rico, San Juan, Puerto Rico 00925-2537, United States*

Bibek Thapa − *Department of Physics, University of Puerto Rico, San Juan, Puerto Rico 00925-2537, United States;* orcid.org/0000-0003-3188-5270

Brad R. Weiner − *Department of Chemistry, University of Puerto Rico, San Juan, Puerto Rico 00925-2537, United States;* orcid.org/0000-0002-5255-1918

Gerardo Morell − *Department of Physics, University of Puerto Rico, San Juan, Puerto Rico 00925-2537, United States;* orcid.org/0000-0003-4787-2239

Wojciech M. Jadwisienczak − *School of Electrical Engineering and Computer Science, Ohio University, Athens, Ohio 45701, United States*

Complete contact information is available at: https://pubs.acs.org/10.1021/acsomega.0c06164

Author Contributions

J.B.-H., M.B., and W.M.J. conceived and designed the project. M.B., B.T., O.G., and D.D.-D. performed in part the experiments. S.S., M.B., and J.B.-H. wrote the article. S.S., O.G., M.B., D.D.-D., B.T., G.M., W.M.J., and J.B.-H. analyzed the data, reviewed, and commented on the article at all stages. All authors read and approved the article.

Funding

J.B.-H. acknowledges the financial support of ECU Research, Economic Development, and Engagement through startup funding. W.M.J. received funding from NSF Cooperative Agreement no. 1002410. G.M. and B.R.W. acknowledge the support from NSF EPSCoR Grant no. OIA-1849243 and NASA EPSCoR Grant no. 80NSSC19M0049.

Notes

The authors declare no competing financial interest.

■ ACKNOWLEDGMENTS

Authors thank the Nanomedicines Characterization Core Facility (NCore) at the Center for Nanotechnology in Drug Delivery (CNDD) at UNC Chapel Hill for ICP−MS analysis. Special thanks to Dr. Ram S. Katiyar for access to his characterization facilities at the University of Puerto Rico, Rio Piedras Campus.

■ REFERENCES

(1) Bsatee, M. *The Development of Experimental Setup for Various Magneto-Optical Studies*; Electronic Thesis & Dissertations Center, Ohio University, 2015; p 105.

(2) Ando, K.; Saito, H.; Jin, Z.; Fukumura, T.; Kawasaki, M.; Matsumoto, Y.; Koinuma, H. Magneto-Optical Properties of ZnO-Based Diluted Magnetic Semiconductors. *J. Appl. Phys.* **2001**, *89*, 7284.

(3) Ando, K.; Saito, H.; Zayets, V.; Debnath, M. C. Optical Properties and Functions of Dilute Magnetic Semiconductors. *J. Phys.: Condens. Matter* **2004**, *16*, S5541−S5548.

(4) Oka, Y.; Kayanuma, K.; Shirotori, S.; Murayama, A.; Souma, I.; Chen, Z. Magneto-Optical Properties and Exciton Dynamics in Diluted Magnetic Semiconductor Nanostructures. *J. Lumin.* **2002**, *100*, 175−190.

(5) Dietl, T. A Ten-Year Perspective on Dilute Magnetic Semiconductors and Oxides. *Nat. Mater.* **2010**, *9*, 965−974.

(6) Wang, Y.; Herron, N.; Moller, K.; Bein, T. Three-Dimensionally Confined Diluted Magnetic Semiconductor Clusters: $Zn_{1-x}Mn_xS$. *Solid State Commun.* **1991**, *77*, 33−38.

(7) Kacman, P. Spin Interactions in Diluted Magnetic Semiconductors and Magnetic Semiconductor Structures. *Semicond. Sci. Technol.* **2001**, *16*, R25−R39.
(8) Archer, P. I.; Santangelo, S. A.; Gamelin, D. R. Direct Observation of sp−d Exchange Interactions in Colloidal Mn^{2+}- and Co^{2+}-Doped CdSe Quantum Dots. *Nano Lett.* **2007**, *7*, 1037−1043.
(9) Gaj, J. A.; Kossut, J. Basic Consequences of sp−d and d−d Interactions in DMS. In: Introduction to the Physics of Diluted Magnetic Semiconductors. *Springer Ser. Mater. Sci.* **2010**, *144*, 1−36.
(10) Chekhovich, E. A.; Brichkin, A. S.; Chernenko, A. V.; Kulakovskii, V. D. Effect of sp-d Exchange Interaction on Excitonic States in CdSe/ZnSe/$Zn_{1-x}Mn_xSe$ Quantum Dots. *Phys. Rev. B: Condens. Matter Mater. Phys.* **2007**, *76*, 165305.
(11) Muckel, F.; Delikanli, S.; Hernández-Martínez, P. L.; Priesner, T.; Lorenz, S.; Ackermann, J.; Sharma, M.; Demir, H. V.; Bacher, G. sp−d Exchange Interactions in Wave Function Engineered Colloidal CdSe/Mn:CdS Hetero-Nanoplatelets. *Nano Lett.* **2018**, *18*, 2047−2053.
(12) Sato, K.; Katayama-Yoshida, H. Ab initio Study on the Magnetism in ZnO-, ZnS-, ZnSe-and ZnTe-Based Diluted Magnetic Semiconductors. *Phys. Status Solidi B* **2002**, *229*, 673−680.
(13) Martínez, B.; Sandiumenge, F.; Balcells, L.; Arbiol, J.; Sibieude, F.; Monty, C. Structure and Magnetic Properties of Co-doped ZnO Nanoparticles. *Phys. Rev. B: Condens. Matter Mater. Phys.* **2005**, *72*, 165202.
(14) Hanif, K. M.; Meulenberg, R. W.; Strouse, G. F. Magnetic Ordering in Doped $Cd_{1-x}Co_xSe$ Diluted Magnetic Quantum Dots. *J. Am. Chem. Soc.* **2002**, *124*, 11495−11502.
(15) Sarkar, I.; Sanyal, M. K.; Takeyama, S.; Kar, S.; Hirayama, H.; Mino, H.; Komori, F.; Biswas, S. Suppression of Mn Photoluminescence in Ferromagnetic State of Mn-doped ZnS Nanocrystals. *Phys. Rev. B: Condens. Matter Mater. Phys.* **2009**, *79*, 054410.
(16) Beltran-Huarac, J.; Wang, J.; Tanaka, H.; Jadwisienczak, W. M.; Weiner, B. R.; Morell, G. Stability of the Mn Photoluminescence in Bifunctional ZnS:0.05Mn Nanoparticles. *J. Appl. Phys.* **2013**, *114*, 053106.
(17) Diaz-Diestra, D.; Thapa, B.; Beltran-Huarac, J.; Weiner, B. R.; Morell, G. L-cysteine Capped ZnS:Mn Quantum Dots for Room-temperature Detection of Dopamine with High Sensitivity and Selectivity. *Biosens. Bioelectron.* **2017**, *87*, 693−700.
(18) Xu, W.; Li, T.; Huang, W.; Luan, Y.; Yang, Y.; Li, S.; Yang, W. A Magnetic Fluorescence Molecularly Imprinted Polymer Sensor with Selectivity for Dibutyl Phthalate via Mn doped ZnS Quantum Dots. *RSC Adv.* **2017**, *7*, 51632−51639.
(19) Manimegalai, D. K.; Manikandan, A.; Moortheswaran, S.; Antony, S. A. Magneto-Optical and Photocatalytic Properties of Magnetically Recyclable $Mn_xZn_{1-x}S$ (x = 0.0, 0.3, and 0.5) Nanocatalysts. *J. Supercond. Novel Magn.* **2015**, *28*, 2755−2766.
(20) Sarkar, I.; Sanyal, M. K.; Kar, S.; Biswas, S.; Banerjee, S.; Chaudhuri, S.; Takeyama, S.; Mino, H.; Komori, F. Ferromagnetism in Zinc Sulfide Nanocrystals: Dependence on Manganese Concentration. *Phys. Rev. B: Condens. Matter Mater. Phys.* **2007**, *75*, 224409.
(21) Beltran-Huarac, J.; Diaz-Diestra, D.; Bsatee, M.; Wang, J.; Jadwisienczak, W. M.; Weiner, B. R.; Morell, G. Novel Magneto-Luminescent Effect in LSMO/ZnS:Mn Nanocomposites at Near-Room Temperature. *Nanotechnology* **2016**, *27*, 085703.
(22) Cheng, S.-J. Theory of Magnetism in Diluted Magnetic Semiconductor Nanocrystals. *Phys. Rev. B: Condens. Matter Mater. Phys.* **2008**, *77*, 115310.
(23) Zhao, D. H.; Chen, J. L.; Li, Y. X.; Wang, L. Y.; Wang, L.; Wu, Y. Q.; Zhou, Y. Y.; Zhuo, S. J.; Zhu, C. Q. Application of L-cysteine-capped nano-ZnS as a fluorescence probe for the determination of proteins. *Anal. Bioanal. Chem.* **2004**, *378*, 811−815.
(24) Nabavinia, M.; Beltran-Huarac, J. Recent Progress in Iron Oxide Nanoparticles as Therapeutic Magnetic Agents for Cancer Treatment and Tissue Engineering. *ACS Appl. Bio Mater.* **2020**, *3*, 8172−8187.
(25) Thapa, B.; Diaz-Diestra, D.; Santiago-Medina, C.; Kumar, N.; Tu, K.; Beltran-Huarac, J.; Jadwisienczak, W. M.; Weiner, B. R.; Morell, G. T1- and T2-weighted Magnetic Resonance Dual Contrast by Single Core Truncated Cubic Iron Oxide Nanoparticles with Abrupt Cellular Internalization and Immune Evasion. *ACS Appl. Bio Mater.* **2018**, *1*, 79−89.
(26) Beltran-Huarac, J.; Guinel, M. J.-F.; Weiner, B. R.; Morell, G. Bifunctional Fe_3O_4/ZnS:Mn Composite Nanoparticles. *Mater. Lett.* **2013**, *98*, 108−111.
(27) Rojas-Pérez, A.; Diaz-Diestra, D.; Frias-Flores, C. B.; Beltran-Huarac, J.; Das, K. C.; Weiner, B. R.; Morell, G.; Díaz-Vázquez, L. M. Catalytic effect of ultrananocrystalline Fe_3O_4 on algal bio-crude production via HTL process. *Nanoscale* **2015**, *7*, 17664−17671.
(28) Thapa, B.; Diaz-Diestra, D.; Beltran-Huarac, J.; Weiner, B. R.; Morell, G. Enhanced MRI T_2 Relaxivity in Contrast-probed Anchor-free PEGylated Iron Oxide Nanoparticles. *Nanoscale Res. Lett.* **2017**, *12*, 312.
(29) Dung, C. T.; Quynh, L. M.; Linh, N. P.; Nam, N. H.; Luong, N. H. Synthesis of ZnS:Mn-Fe_3O_4 Bifunctional Nanoparticles by Inverse Microemulsion Method. *J. Sci.: Adv. Mater. Devices* **2016**, *1*, 200−203.
(30) Shan, Y.; Xu, J.-J.; Chen, H.-Y. Opto-Magnetic Interaction between Electrochemiluminescent CdS:Mn Film and Fe_3O_4 Nanoparticles and its Application to Immunosensing. *Chem. Commun.* **2010**, *46*, 4187−4189.
(31) Beltran-Huarac, J.; Martinez, R.; Morell, G. Physical Properties of Bifunctional BST/LSMO Nanocomposites. *J. Appl. Phys.* **2014**, *115*, 084102.
(32) Stefan, M.; Pana, O.; Leostean, C.; Bele, C.; Silipas, D.; Senila, M.; Gautron, E. Synthesis and Characterization of Fe_3O_4−TiO_2 Core-Shell Nanoparticles. *J. Appl. Phys.* **2014**, *116*, 114312.
(33) Stefan, M.; Leostean, C.; Pana, O.; Soran, M.-L.; Suciu, R. C.; Gautron, E.; Chauvet, O. Synthesis and Characterization of Fe_3O_4@ZnS and Fe_3O_4@Au@ZnS core−shell nanoparticles. *Appl. Surf. Sci.* **2014**, *288*, 180−192.
(34) Singh, D. P.; Daoudi, A.; Gupta, S. K.; Pandey, S.; Vimal, T.; Manohar, R.; Kole, A. K.; Kumbhakar, P.; Kumar, A. Mn2+ Doped ZnS Quantum Dots in Ferroelectric Liquid Crystal Matrix: Analysis of New Relaxation Phenomenon, Faster Optical Response, and Concentration Dependent Quenching in Photoluminescence. *J. Appl. Phys.* **2016**, *119*, 094101.
(35) Shrivastava, N.; Khan, L. U.; Khan, Z. U.; Vargas, J. M.; Moscoso-Londoño, O.; Ospina, C.; Brito, H. F.; Javed, Y.; Felinto, M. C. F. C.; Menezes, A. S.; Knobel, M.; Sharma, S. K. Building Block Magneto-Luminescent Nanomaterials of Iron-Oxide/ZnS@LaF_3:Ce^{3+}, Gd^{3+}, Tb^{3+} with green emission. *J. Mater. Chem. C* **2017**, *5*, 2282−2290.
(36) Roychowdhury, A.; Pati, S. P.; Kumar, S.; Das, D. Tunable Properties of Magneto-Optical Fe_3O_4/CdS Nanocomposites on Size Variation of the Magnetic Component. *Mater. Chem. Phys.* **2015**, *151*, 105−111.
(37) Shen, B.; Zhou, H.; Chen, Z.; Wang, Z.; Sheng, Y.; Chen, J.; Geng, B. Synthesis and Optoelectrochemical Properties of ZnS:Mn Nanocrystals. *J. Nanosci. Nanotechnol.* **2012**, *12*, 3931.
(38) Bragg, W. H. The Structure of Magnetite and the Spinels. *Nature* **1915**, *95*, 561.
(39) Huang, H. Y.; Chen, Z. Y.; Wang, R.-P.; de Groot, F. M. F.; Wu, W. B.; Okamoto, J.; Chainani, A.; Singh, A.; Li, Z.-Y.; Zhou, J.-S.; Jeng, H.-T.; Guo, G. Y.; Park, J.-G.; Tjeng, L. H.; Chen, C. T.; Huang, D. J. Jahn-Teller Distortion Driven Magnetic Polarons in Magnetite. *Nat. Commun.* **2017**, *8*, 15929.
(40) Diaz-Diestra, D.; Thapa, B.; Badillo-Diaz, D.; Beltran-Huarac, J.; Morell, G.; Weiner, B. Graphene Oxide/ZnS:Mn Nanocomposite Functionalized with Folic Acid as a Nontoxic and Effective Theranostic Platform for Breast Cancer Treatment. *Nanomaterials* **2018**, *8*, 484.
(41) Kumbhakar, P.; Sarkar, R.; Mitra, A. K. Synthesis and optical properties of L-cystine capped ZnS:Co Nanoparticles. *NSTI-Nanotech* **2010**, *1*, 530−533.

https://dx.doi.org/10.1021/acsomega.0c06164
ACS Omega 2021, 6, 7598−7604